Supplementary file

Organic-inorganic pore evolution modeling in natural lacustrine shale influenced by mineral composition: Implications for shale oil exploration and CO_2 storage

Liu Wang[1,2], Bo Liu[1*], Longhui Bai[1], Zhichao Yu[3], Qiuli Huo[4] , YiFei Gao[1,2]

[1] *Sanya Offshore Oil & Gas Research Institute, Northeast Petroleum University, Sanya 572025, P. R. China*

[2] *National Key Laboratory of Continental Shale Oil, Northeast Petroleum University, Daqing 163318, P. R. China*

[3] *PetroChina Exploration and Development Research Institute, Beijing 100083, P. R. China*

[4] *Daqing Oilfield Company of CNPC, Daqing 163000, P. R. China*

E-mail address: wangliu_nepu@163.com (L. Wang); liubo@nepu.edu.cn (B. Liu); bailonghui0302@163.com (L. Bai); yuzhichao@petrochina.com.cn (Z. Yu); huoql@petrochina.com.cn (Q. Huo); gaoyifei1999@outlook.com (Y. Gao).

[*] Corresponding author (ORCID: 0000-0003-0136-7237)

Wang, L., Liu, B., Bai, L., Yu, Z., Huo, Q., Gao, Y. Organic-inorganic pore evolution modeling in natural lacustrine shale influenced by mineral composition: Implications for shale oil exploration and CO_2 storage. Advances in Geo-Energy Research, 2024, 13(3): 218-230.

The link to this file is: https://doi.org/10.46690/ager.2024.09.07

Geological setting

The Songliao Basin is a large, north-northeast-trending and rhombus-shaped continental sedimentary basin, which contains six first-order structural units (Wang et al., 2022; Zhou et al., 2022) (Fig. S1(a)). The Qingshankou Formation is dominated by lake deposits under warm and humid conditions and developed during a rapid, large-scale lake transgression, which belongs to the deep to semi-deep lake sedimentary environment. It deposited a set of widely covered dark shale with a thickness around 100 meters (Fig. S1(c)), The content of total organic carbon (TOC) contents in the Qingshankou Formation ranges from 1.4 to 2.5wt.%. The kerogen types mainly include type I and type II_1, which is a typical oil-prone, organic-rich lacustrine shales. The vitrinite reflectance (R_o) of the Qingshankou Formation ranges from 0.5% to 2.0% (Liu et al., 2022). The study area includes Qijia-Gulong Sag, southern area of Daqing Placanticline and Sanzhao Sag (Fig. S1(b)).

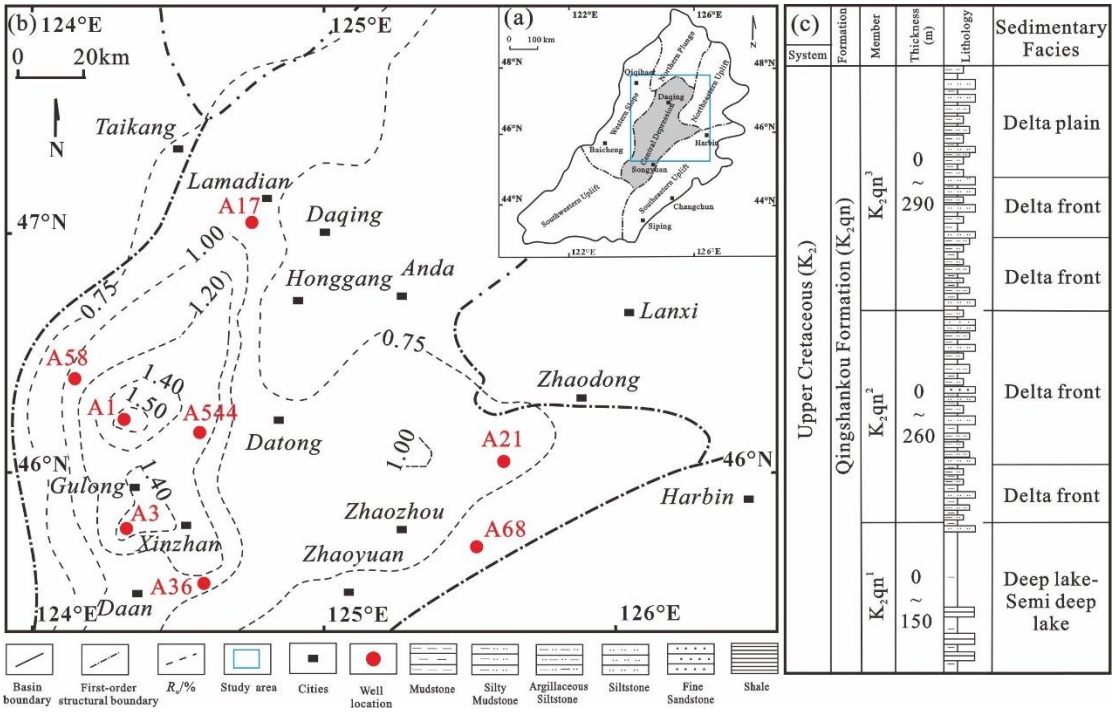

Fig. S1. Location and stratigraphic column of the study area. (a) Location of study area in the northern Songliao Basin, (b) geological map of the study area showing sampling well locations and (c) stratigraphic sequences in northern the (modified from Liu et al., 2023).

X-ray diffraction analysis (XRD) and TOC

The mineral compositions were tested by Bruker D8 Advance goniometer X-ray diffractometer. First, the samples were ground and sieved to a grain size less than 0.15 mm, and then conducted X-ray diffraction. The position of the diffraction peak is related to the mineral type, and the intensity of the diffraction peak is related to the mineral content. Then, using the semi-quantitative principle to calculate the content of different mineral components in the sample. The TOC was detected by Eltra Helios CS elemental analyzer. Samples were pretreated with phosphoric acid to remove carbonates.

Optical observation and field emission scanning electron microscope (FE-SEM)

To investigate the pore and diagenetic types of the samples, a Apreo FE-SEM machine was used to perform SEM imaging together with back scattered electron (BSE) mode. Combined with the equipped Bruker energy spectrometer to perform qualitative or semi-quantitative micro-area component analysis. The SEM work was carried out with 5 keV accelerating voltage and 0.4 nA current, the working distance is 4 mm. MAPS images were acquired using the Apreo high-resolution FE-SEM. Each Maps contain 750 photographs. Use edge-threshold automatic processing (ETAP) technology to count the percentages of organic pores, inorganic pores, organic cracks and inorganic cracks of the Maps images. An automatic shale porosity quantification method using an ETAP technique from Tian et al. (2021) was applied. After that, the pore identification system V1.0 was used to calculate the organic pore rate, inorganic pore rate and total surface porosity respectively. Various charts from image processing included montaged high resolution SEM images and extracted images of organic and inorganic pores can be found in Liu et al. (2023).

Low temperature nitrogen adsorption (LN_2A) and mercury intrusion capillary pressure (MICP)

The LN_2A was completed on the American Mike ASAP2640 fully automatic specific surface

area (SSA) and pore size analyzer. The sample was crushed to 60-80 mesh, and then degassed in a vacuum at 110 °C for at least 14 hours to remove residual gas and adsorbed water, the adsorption and desorption curves are measured after drying. In this study, the BET model was used to obtain the SSA, the BJH model was used to obtain pore volume and average pore diameter, and the DFT model was used to obtain the pore size distribution characteristics. The MICP was completed on the Micromeritics Auto pore 9520 with a maximum pressure of 60,000 psi (414 MPa). The standard process of following the procedure described by Sun et al. (2022).

Table S1. Mineralogical compositions and organic geochemical data of shale samples for the Qingshankou Formation in the Songliao Basin.

No.	Depth (m)	R_o (%)	Lithofacies	TOC (wt.%)	Mineral composition (%)								
					Quartz	K-feldspar	Plagioclase	Calcite	Ankerite	Dolomite	Siderite	Pyrite	Clay
A68-01	1,107.58	0.6	Calcareous shale	2.44	17.2	0.0	4.5	0.0	0.0	55	0.0	11.4	11.9
A68-02	1,135.32	0.62	Argillaceous shale	5.91	34.0	1.5	15.3	5.3	0.0	0.0	0.0	2.6	41.3
A21-01	1,627.03	0.8	Calcareous shale	2.96	16.1	4.5	7.4	0.4	46.9	0.0	0.0	1.7	22.9
A21-02	1,635.63	0.72	Mixed shale	2.91	34.6	1.4	14.5	0.0	6.7	0.0	2.8	2.2	37.8
A21-03	1,659.45	0.83	Mixed shale	3.01	39.7	0.0	12.9	6.3	0.0	0.0	0.0	3.1	38.0
A21-04	1,664.95	0.84	Felsic shale	4.64	48.6	0.0	17.1	0.0	0.0	0.0	0.0	4.5	29.8
A17-01	2,014.66	0.95	Mixed shale	1.35	32.0	0.0	12.4	10.8	13.6	0.0	0.0	2.5	28.8
A17-02	2,289.01	1.01	Felsic shale	2.01	34.2	4.0	24.8	2.9	0.0	0.0	3.1	3.8	27.3
A17-03	2,371.57	0.89	Argillaceous shale	2.10	32.8	1.6	20.4	0.0	0.0	0.0	2.6	0.0	42.6
A17-04	2,405.90	1.02	Argillaceous shale	2.02	33.6	0.0	11.9	7.6	0.0	0.0	0.0	6.3	40.6
A58-01	2,047.01	1.15	Mixed shale	2.43	31.9	0.0	17.9	3.0	2.3	0.0	2.0	3.2	39.8
A58-02	2,048.35	1.16	Calcareous shale	0.55	17.4	6.9	30.5	40.0	0.0	0.0	0.0	1.7	3.4
A58-03	2,068.69	1.17	Argillaceous shale	2.55	32.2	1.6	20.6	0.0	0.0	0.0	0.8	2.7	42.1

(continued on next page)

Table 1 (*continued*)

A36-01	2,212.87	1.33	Argillaceous shale	2.93	24.9	0.0	15.3	0.0	7.6	0.0	0.0	4.4	47.8
A36-02	2,260.40	1.36	Felsic shale	1.47	37.1	0.0	23.2	9.7	0.0	0.0	1.0	3.5	25.6
A554-01	2,237.37	1.21	Argillaceous shale	2.19	33.1	0.9	14.9	0.0	0.0	0.0	0.0	4.0	47.1
A554-02	2,250.69	1.22	Argillaceous shale	2.22	37.8	0.0	12.7	0.0	0.0	0.0	0.0	0.0	49.4
A554-03	2,281.15	1.25	Mixed shale	1.68	35.9	0.0	10.6	11.2	0.0	0.0	0.0	4.9	37.4
A3-01	2,431.00	1.41	Mixed shale	2.65	33.9	1.1	19.6	1.3	0.0	0.0	1.5	4.9	37.7
A3-02	2,449.50	1.41	Mixed shale	1.59	27.4	1.3	14.0	2.0	18.6	0.0	0.0	1.8	34.8
A3-03	2,455.70	1.43	Mixed shale	2.28	27.1	0.9	24.7	7.3	0.0	0.0	0.7	3.5	35.9
A3-04	2,468.90	1.43	Mixed shale	2.45	30.3	0.0	15.6	0.0	13.1	0.0	3.4	3.7	33.9
A3-05	2,471.80	1.42	Argillaceous shale	2.43	27.6	0.0	17.1	0.0	10.6	0.0	0.6	2.6	41.6
A1-01	2,530.92	1.6	Mixed shale	2.13	27.6	0.0	13.3	4.9	19.6	0.0	0.0	3.3	31.4
A1-02	2,532.62	1.61	Felsic shale	1.81	35.5	2.2	23.2	7.4	0.0	0.0	0.0	2.1	29.6
A1-03	2,534.52	1.6	Mixed shale	2.17	29.5	1.3	11.3	2.2	15.2	0.0	0.0	1.8	38.9
A1-04	2,538.12	1.62	Felsic shale	4.08	34.2	1.1	21.5	0.9	4.4	0.0	0.0	0.8	37.1
A1-05	2,545.41	1.64	Felsic shale	2.73	35.4	1.3	19.0	0.0	6.6	0.0	0.0	3.6	34.1
A1-06	2,549.66	1.66	Felsic shale	1.94	36.8	1.8	21.3	0.8	0.0	0.0	0.0	1.1	38.1
A1-07	2,555.66	1.67	Argillaceous shale	2.39	32.1	1.0	19.9	1.7	2.4	0.0	0.0	2.6	40.3

Table S2. Percentage of different pore types of shale samples obtained from automatic porosity quantification.

No.	OM pores (%)	OM cracks (%)	Intraparticle pores (%)	Interparticle pores (%)	Intercrystal pores (%)	Inorganic cracks (%)	OM surface porosity (%)	Inorganic surface porosity (%)	Total surface porosity (%)	Organic pore ratio (%)	Inorganic pore ratio (%)
A68-01	2	1	19	39	23	16	0.067	0.342	0.409	16.38	83.62
A68-02	5	8	19	25	24	19	0.089	0.345	0.434	20.51	79.49
A21-01	1	1	32	25	23	18	0.034	0.269	0.304	11.35	88.65
A21-02	9	9	17	23	26	16	0.152	0.483	0.635	23.92	76.08
A21-04	10	16	12	29	24	9	0.074	0.042	0.116	63.98	36.02
A58-02	1	1	23	31	39	5	0.007	0.406	0.413	1.69	98.31
A36-02	19	7	10	24	26	14	0.201	0.487	0.688	29.23	70.77
A554-02	18	10	15	14	25	18	0.037	0.701	0.739	5.07	94.93
A3-05	20	6	13	22	19	20	0.227	0.709	0.937	24.28	75.72
A1-02	10	1	27	26	29	7	0.066	0.583	0.649	10.17	89.83
A1-03	7	1	21	30	39	2	0.036	0.426	0.462	7.79	92.21
A1-07	24	1	11	24	21	19	0.154	0.485	0.639	24.10	75.90

References

Liu, B., Wang, L., Fu, X., et al. Identification, evolution and geological indications of solid bitumen in shales: A case study of the first member of Cretaceous Qingshankou Formation in Songliao Basin, NE China. Petroleum Exploration and Development, 2023, 50(6): 1345-1357.

Liu, B., Wang, Y., Tian, S., et al. Impact of thermal maturity on the diagenesis and porosity of lacustrine oil-prone shales: Insights from natural shale samples with thermal maturation in the oil generation window. International Journal of Coal Geology, 2022, 261: 104079.

Sun, M., Wen, J., Pan, Z., et al. Pore accessibility by wettable fluids in overmature marine shales of China: Investigations from contrast-matching small-angle neutron scattering (CM-SANS). International Journal of Coal Geology, 2022, 255: 103987.

Tian, S., Bowen, L., Liu B., et al. A method for automatic shale porosity quantification using an Edge-Threshold Automatic Processing (ETAP) technique. Fuel, 2021, 304: 121319.

Wang, B., Liu, B., Yang, J., et al. Compatibility characteristics of fracturing fluid and shale oil reservoir: a case study of the first member of Qingshankou Formation, northern Songliao Basin, Northeast China. Journal of Petroleum Science and Engineering, 2022, 211: 110161.

Zhou, J., Liu, B., Shao, M., et al. Lithologic classification of pyroclastic rocks: A case study for the third member of the Huoshiling Formation, Dehui fault depression,

Songliao Basin, NE China. Journal of Petroleum Science and Engineering, 2022, 214: 110456.